2007-03-28

Comparison of Stent Designs using Computational Fluid Dynamics

Jonathan Murphy
Dublin Institute of Technology, jonathan.murphy@dit.ie

Fergal Boyle
Dublin Institute of Technology, fergal.boyle@dit.ie

Comparison of Stent Designs Using Computational Fluid Dynamics

Jonathan Murphy, Fergal Boyle
Department of Mechanical Engineering
Dublin Institute of Technology
Bolton Street, Dublin 1

Abstract

Coronary artery disease (CAD) is one of the leading causes of death in the developed world. CAD occurs due to the build up of plaque in the coronary arteries which supply fresh blood to the constantly active heart muscle. Several methods exist to alleviate CAD such as coronary artery bypass grafting, balloon angioplasty and coronary stenting. A coronary stent is a small tubular prosthesis which can improve blood flow by acting as a scaffold to prop the diseased artery open. However, stent restenosis (re-blockage) remains a common problem with different stent designs leading to different restenosis rates. This work investigates a relationship between restenosis and the induced flow fields for two different stent designs. Two models have been developed using advanced computational fluid dynamics (CFD) in order to assess the haemodynamic impact of coronary stent implantation. One model represents the left anterior descending (LAD) coronary artery implanted with a Palmaz-Schatz (PS) stent and the second model represents the same artery implanted with a Gianturco-Roubin-II (GR-II) stent. Mathematical models were constructed to simulate the fully developed, non-Newtonian nature of the coronary blood flow. Two flow characteristics that are known to encourage restenosis are low wall shear stress (WSS) and high wall shear stress gradient (WSSG) and both have been identified from the computational simulations. Using data from a recent clinical restenosis trial of the GR-II stent and the PS stent, correlations between flow characteristics and restenosis rates have been investigated.

1. Introduction

Atherosclerosis is a disease affecting the arterial blood vessel in which an atheromatous plaque forms on the wall of the vessel and restricts the flow of blood. When atherosclerosis occurs in the coronary arteries which perfuse the heart muscle the condition is known as CAD. In the past a coronary artery bypass graft was the only treatment available for CAD. This is a large scale operation involving the sawing open of the breastbone and grafting of a blood vessel to bypass the site of the blockage.

Percutaneous transluminal coronary angioplasty (PTCA) was introduced in the late 1970s as a minimally invasive procedure to relieve the narrowing in a coronary artery due to the build up of plaque. PTCA is accomplished with a small balloon catheter inserted into an artery in the groin or arm, and advanced to the narrowing in the coronary artery. The balloon is then inflated to enlarge the narrowing in the artery and restore blood flow to the heart muscle. However in over 40% of

patients treated with PTCA the artery becomes re-blocked within six months in a process known as restenosis [1]. This is largely due to elastic recoil of the vessel wall [2].

In the early 1990s stents were introduced to improve the success rates of PTCA. Basically, a stent is an expandable, slotted metal tube inserted into the artery. It acts as a scaffold to provide support for the artery and has proven effective at eliminating elastic recoil, one mechanism of restenosis that can result in re-blockage [2]. The use of stents has shown more promising clinical outcomes than PTCA alone. However, restenosis remains a persistent problem with restenosis rates generally as high as 20% at six months after intervention [3].

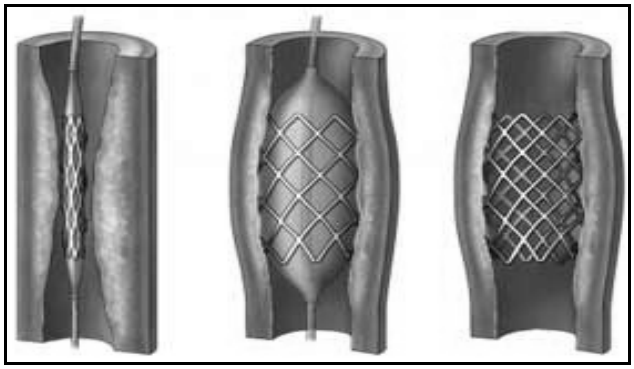

Figure 1: The stenting procedure for a narrowed artery.

The changes in WSS induced by an implanted stent play a significant role in the immunological behaviour of the coronary artery. This behaviour is directly linked to restenosis within the stented artery [4, 5]. In order to assess the haemodynamic impact of coronary stent implantation, three-dimensional computational models of a stented LAD coronary artery have been created using computer-aided-design. One model represents the artery implanted with a PS stent and the second model represents the artery implanted with a GR-II stent. CFD was used to simulate the flow field of the coronary artery with the implanted stent in each case.

Results are shown of the mesh convergence studies conducted. Contour plots and graphs of areas of high and low WSS and a graph of the axial WSSG in the vicinity of struts for both stents are also presented. The GR-II stent has been shown to perform poorly against the PS stent in a recent medical trial. The CFD results presented suggest that this poor performance may be directly linked to the stent induced haemodynamic factors.

2. Materials and Methods

2.1 Introduction

Many different stent designs exist on the market today, each with its own unique geometry. It has been shown that the type of stent used to treat a blockage is a predominant factor affecting restenosis [6]. It is also clear that each particular stent design will have a different effect on the haemodynamics of the blood flowing through it. This study uses CFD to quantitatively compare the haemodynamic effects of two different realistic stent designs and compares those effects to restenosis rates.

2.2 Geometry

The two stent designs modelled using CFD are shown in Figures 2(a) and 2(b) below. The first is the PS coronary stent manufactured by Johnson and Johnson. The stent is 15 mm long, consisting of two 7 mm sections joined by a 1 mm bridge; it ranges from 3 mm to 4 mm in diameter and is a slotted tube balloon expandable design. The stent wires have a rectangular cross section measuring 0.13 mm in width and 0.06mm in thickness. The second type of stent is the GR-II which is manufactured by Cook. The GR-II stent has a balloon expandable coil design and is produced in 20 mm and 40 mm lengths ranging from 2.5 mm to 4 mm in diameter. It also has a rectangular cross section of 0.076 mm in thickness and 0.172 mm in width.

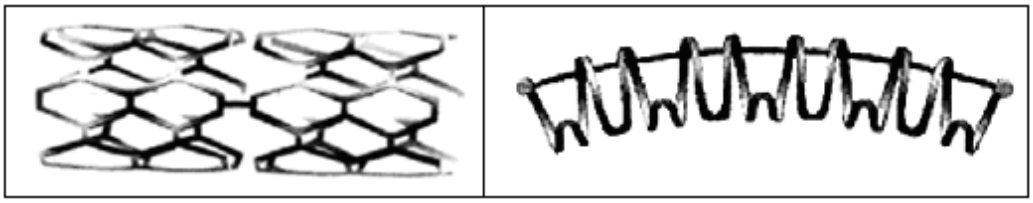

Figure 2(a): The Palmaz-Schatz stent developed by Johnson and Johnson and (b): The Gianturco-Roubin II stent developed by Cook.

In both computational models a cylindrical domain was created and the stent design cut from the domain to simulate conditions of the stent semi-embedded in the artery wall. One of the 7 mm sections of the PS stent was modelled and a half section of the 20 mm long GR-II stent was modelled. The domain extended 2.5 mm proximal (upstream) and 2.5 mm distal (downstream) of the stent in each case to capture the flow field in those regions.

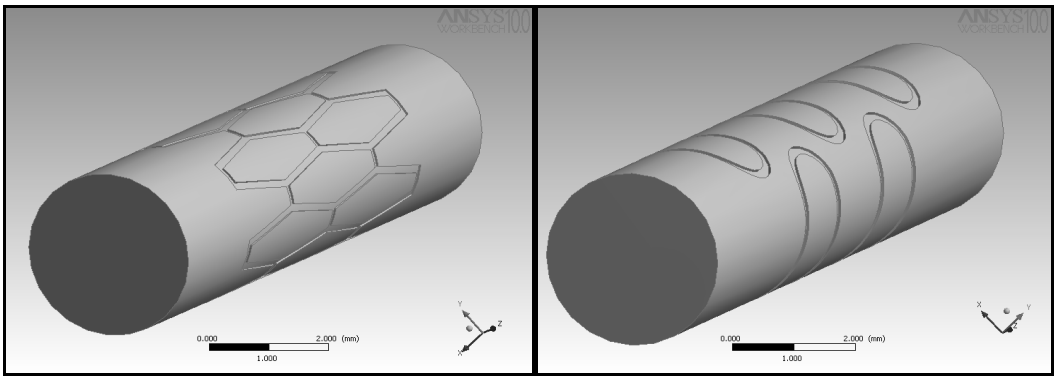

Figure 3: Computational domain representing the left anterior descending coronary artery with implanted (a) PS stent and (b) Gianturco-Roubin II stent

2.3 Computational Fluid Dynamics

CFD is a process whereby real-life fluid flows are simulated using numerical methods to solve the governing equations of fluid dynamics. CFD is a relatively new branch of fluid dynamics commonly regarded as the "third" technique for solution of fluid flow problems, complementing, but not replacing the well-established approaches of theory and experiment. CFD finds it niche in modelling fluid flows that are difficult or impossible to model using theory and are complex, time consuming or expensive to measure experimentally.

2.4 Governing Equations of Fluid Mechanics

Both simulations involved steady laminar flow which requires the CFD code to solve the conservation of mass and momentum equations, of which the general form are listed as Equations (1) and (2) respectively:

$$\frac{\partial \rho}{\partial t} + \nabla.\left(\rho \vec{V}\right) = 0 \tag{1}$$

$$\frac{\partial \rho \vec{V}}{\partial t} + \nabla.\left(\rho \vec{V} \otimes \vec{V}\right) = -\vec{\nabla} p + \vec{\nabla}.(\tau) + \rho \vec{g} + \vec{F} \tag{2}$$

where ρ is the fluid density, p is the static pressure, $\vec{V}$ is the velocity vector, $\vec{F}$ represents external body forces such as gravity, μ is the fluid dynamic viscosity and τ is the shear stress tensor given by Equation (3):

$$\tau = \mu\left(\nabla\vec{V} + \nabla\vec{V}^{T}\right) \tag{3}$$

At low shear rates blood exhibits the non-Newtonian behaviour of variable dynamic viscosity which is dependant on the shear rate. The non-Newtonian nature of the flow is accommodated by using the Carreau model [7] given in Equation (4):

$$\mu = \mu_{\infty} + (\mu_0 - \mu_{\infty})\left[1 + (\gamma\lambda)^2\right]^{\left(\frac{q-1}{2}\right)} \tag{4}$$

where γ is the rate of deformation tensor given by Equation (5) for a three-dimensional Cartesian coordinate system

$$\gamma = \left[\begin{array}{l} 2\left\{\left(\frac{\partial v_x}{\partial x}\right)^2 + \left(\frac{\partial v_y}{\partial y}\right)^2 + \left(\frac{\partial v_z}{\partial z}\right)^2\right\} \\ + \left(\frac{\partial v_x}{\partial y} + \frac{\partial v_y}{\partial x}\right)^2 + \left(\frac{\partial v_x}{\partial z} + \frac{\partial v_z}{\partial x}\right)^2 + \left(\frac{\partial v_y}{\partial z} + \frac{\partial v_z}{\partial y}\right)^2 \end{array}\right]^{\frac{1}{2}} \tag{5}$$

and the constants for the Carreau model given below have been established from experimental data [7]:

$$\begin{array}{ll} \mu_0 = 0.056 \text{ Pa.s} & \lambda = 3.31 \text{ s} \\ \mu_{\infty} = 0.00345 \text{ Pa.s} & q = 0.375 \end{array} \tag{6}$$

The highly sophisticated commercial software code CFX^{TM} was used to solve the governing equations of fluid mechanics for non-Newtonian blood flow in the computational domain using a vertex-centred finite volume scheme.

2.5 Boundary Conditions

The same boundary conditions were applied at the inlet, outlet and on the walls for both simulations. A fully developed axial velocity profile was applied at the inlets given by:

$$V = V_{Max}\left(1 - \frac{r^2}{R^2}\right) \tag{7}$$

where the variable r is the radius measured from the centreline at any point on the inlet plane and R is the radius at the wall of the domain. V_{Max} is the maximum centreline velocity given a value of 0.412 m/s in Equation (7) to simulate resting conditions in the LAD coronary artery [8]. A static pressure of zero Pascals was applied at the outlets of the both domains, allowing the software to calculate the velocity at these planes. The no-slip boundary condition was applied on all surfaces representative of the artery wall and the stent wires.

2.6 Computational Mesh

Analytical solutions to the governing equations of fluid mechanics exist for only the simplest of flows under ideal conditions. To obtain solutions for real flows a numerical approach must be adopted whereby the equations are replaced by algebraic approximations which may be solved using a numerical method. To achieve this, the computational domain must be divided into a set of much smaller non-overlapping sub-domains called elements which constitute the mesh. To obtain an accurate solution a sufficient number of elements must be placed in the computational domain. Figure 4 shows the fine mesh employed in the area around the PS stent wires.

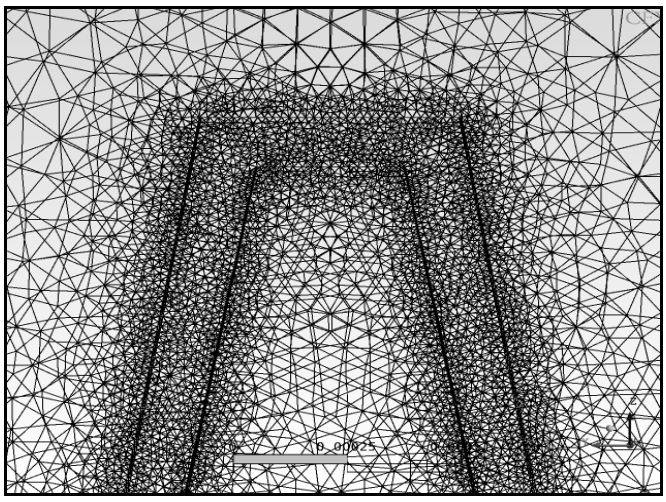

Figure 4: Computational mesh of tetrahedral elements representing the domain in the vicinity of a PS stent strut.

3. Results

3.1 Mesh Convergence Study

A mesh convergence study was carried out to establish the required mesh density for accurate solutions, such that any increase in nodes would lead to no appreciable difference in the solution. Mesh convergence was achieved for both simulations by sequentially increasing the number of nodes until there was no appreciable difference in the axial distribution of WSS across one of the stent struts between the solutions.

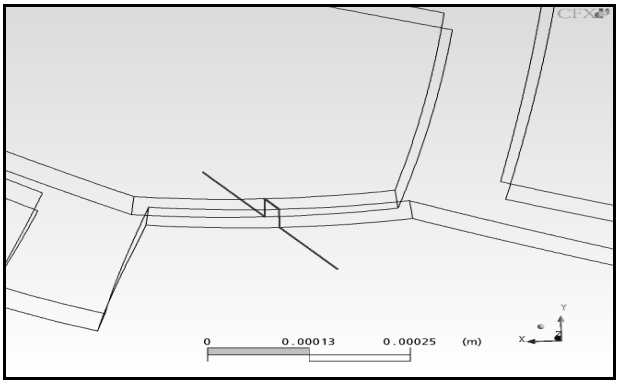

Figure 5: PS Stent strut and sample line upon which mesh convergence study was carried out.

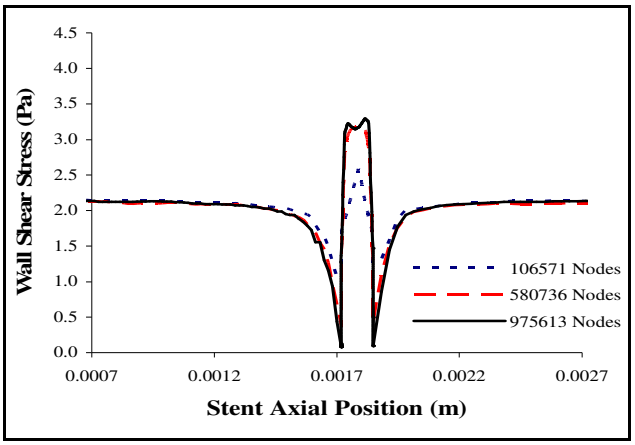

Figure 6: Axial distributions of WSS across a PS stent strut as calculated by successively refined computational meshes.

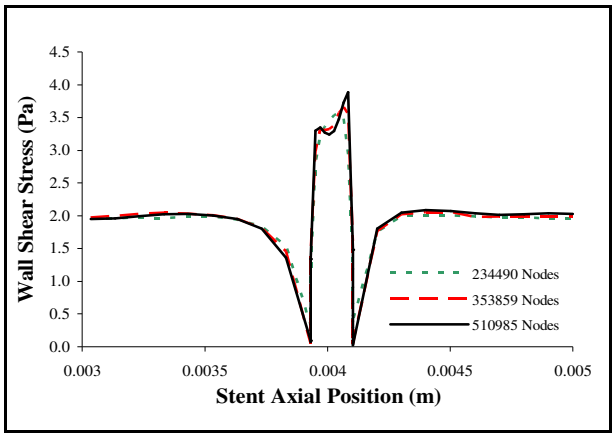

Figure 7: Axial distributions of WSS across a GR-II stent strut as calculated by successively refined computational meshes.

3.2 Wall Shear Stress Results

The predicted three-dimensional flow field reveals areas of high WSS on the tops of the stent struts and low WSS immediately proximal and distal to the stent struts, particularly those transversal to the blood flow as shown in Figures 8 and 9. Figure 10 illustrates the percentage stented area subjected to WSS below a given magnitude starting from 0.1 Pascals. In comparison to the PS stent, the GR-II stent has more than double the percentage stented area subjected to WSS less than 0.1 and 0.25 Pascals, and approximately 70% more percentage stented area subjected to less than 0.5 Pascals. The GR-II stent also has areas on the stent wires with higher WSS than the PS stent with a maximum WSS value of 4.28 Pascals compared to the PS stent which has a maximum of 3.73 Pascals.

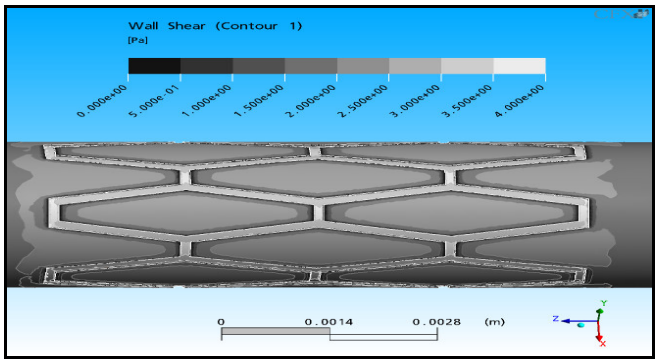

Figure 8: Contour map of WSS in the vicinity of the implanted PS coronary stent.

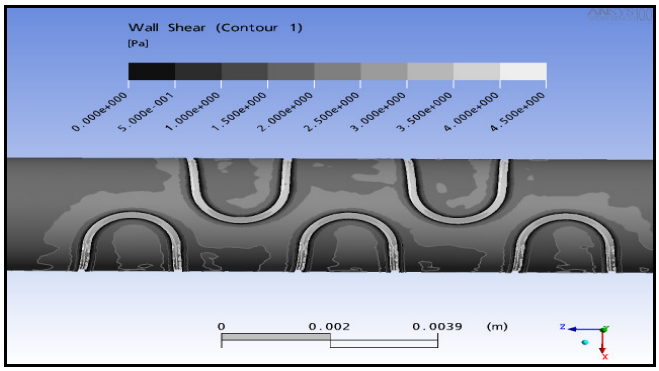

Figure 9: Contour map of WSS in the vicinity of implanted GR-II coronary stent.

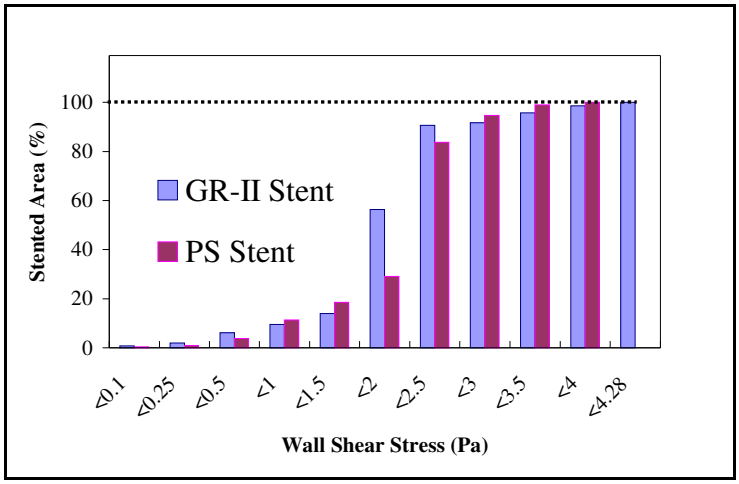

Figure 10: Bar chart illustrating percentage stented area subjected to varying degrees of WSS for the GR-II and PS stent.

Figures 11 and 12 graphically illustrate the axial distribution of WSS and WSSG over one stent strut transversal to the flow direction which is where the maximum WSSG appears as shown in Figures 8 and 9. The magnitude of low WSS on both sides of the strut is similar for both stents. However, the GR-II stent displays 15% higher WSS on the top of the stent strut than the PS stent leading to a 21% higher WSSG in front of the stent strut and a 44% increase in WSSG behind the strut.

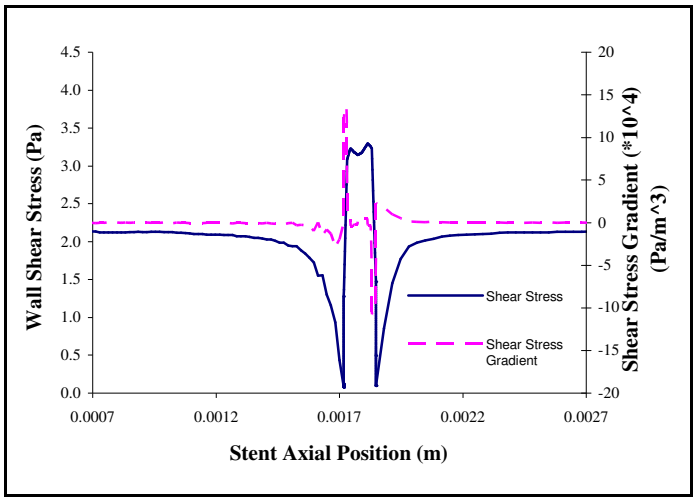

Figure 11: Distribution of WSS and WSSG in the axial direction over one of the PS stent struts.

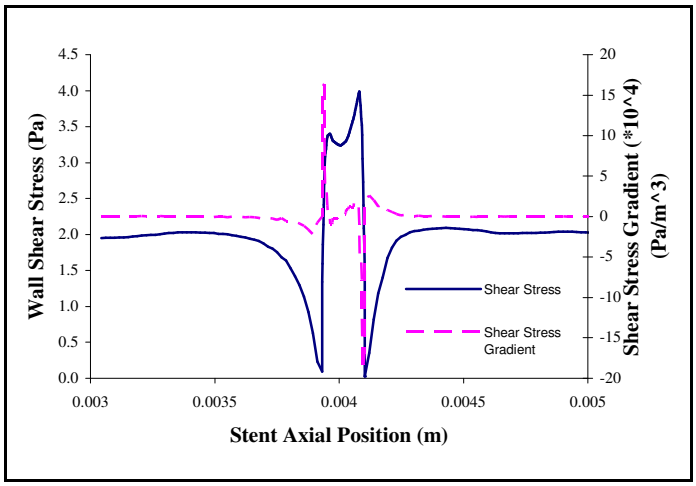

Figure 12: Distribution of WSS and WSSG in the axial direction over one of the GR-II stent struts.

4. Discussion

Endothelial cells (EC) line the interior surface of the blood vessel and are sensitive to stresses exerted on them by the blood flow. Platelets flow in the blood stream and are responsible for the formation of blood clots at the site of arterial injuries. Restenosis occurs in a stented artery when the smooth muscle cells shown in Figure 13 migrate to the vessel lumen from the media and restrict the blood flow. Smooth muscle cells will migrate when signalled by platelets, EC or a

combination of both. EC and platelets will signal smooth muscle cells when subjected to arterial injury or abnormal stresses from the blood flow. The accumulation of smooth muscle cells on the inner surface of the arterial wall is termed neointimal hyperplasia (NH)

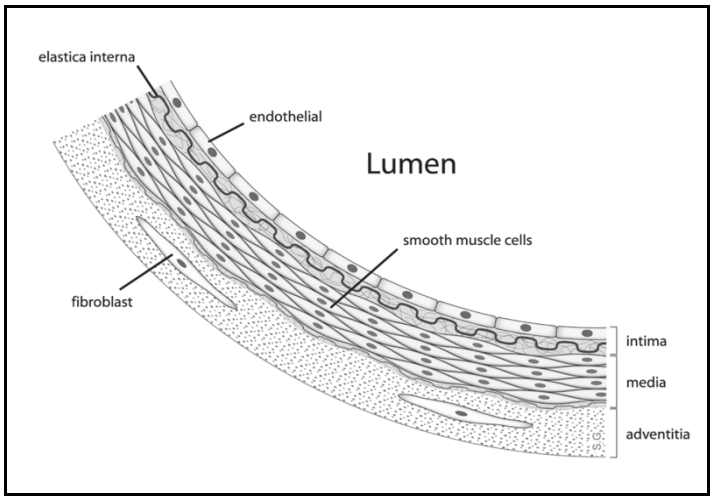

Figure 13: A cross sectional view of part of the artery wall.

4.1 Arterial Injury

EC will be injured to some extent by the stenting procedure and this will signal the smooth muscle cells. It has been established that the magnitude of the arterial injury determines the amount of NH that will occur [9]. The signalling process will continue until the damaged cells are replaced by new endothelium.

4.2 Wall Shear Stress

Regions of low WSS in an artery lead to an increase in NH via two mechanisms. Firstly, EC subjected to WSS below 0.5 N/m^2 will produce substances which will signal smooth muscle cells [10]. Secondly, it has been shown that platelet deposition and residence times are higher in regions of low WSS and that platelets have the ability to signal smooth muscle cells [11, 12]. The results show that the artery implanted with the GR-II stent has 6.1% of its stented area subjected to WSS below 0.5 N/m^2 immediately after stent implantation, compared to 3.7% with the PS stent. This larger area exposed to the critical range of low WSS would make the GR-II stent more prone to NH formation and hence, restenosis.

4.3 Wall Shear Stress Gradients

The success of a stenting procedure relies heavily on the re-endothelialisation of the vessel wall after implantation and the successful function of the newly formed EC to inhibit platelet deposition. If a new layer of EC successfully grows over the stent the NH formation will be attenuated [13]. It has been shown that endothelial cells will migrate away from areas of high WSSG [14]. Through the inhibition of reendothelialisation, high WSSG contribute to NH formation. The results show that both stents set up high WSSG around the stent wires, however the GR-II stent has up to 44% higher WSSG than the PS stent. This would lead to less chance of a successful re-endothelialisation of the area around the stent wires, encouraging restenosis.

5. Conclusion

It is clear that haemodynamics of the flow in an artery implanted with a stent have an effect on the immunological response within the vessel wall of that artery. This work has demonstrated that stent design has an effect on those haemodynamic characteristics.

In a medical trial conducted to compare the in vivo performance of these two stents, the GR-II stent had a restenosis rate of 47.3% compared to the PS restenosis rate of 20.6% after six months [15]. Areas of low WSS and high WSSG have earlier been identified as factors which encourage the development of NH which leads to restenosis. The CFD results predict that implantation of the GR-II stent rather than the PS stent would produce more of these restenosis prone haemodynamic effects in the stented artery. The medical trial data and predicted CFD results correlate strongly to suggest that coronary haemodynamics due to stent design are a significant factor in whether or not the stenting procedure will be successful. In light of this evidence, future stent designs should strive to reduce restenosis encouraging haemodynamic effects, primarily regions of low WSS and high WSSG.

References

[1] D. L. Fischman, M. B. Leon, & D. S. Baim, *A Randomized Comparison of Coronary Stent Placement and Balloon Angioplasty in Treatment of Coronary Artery Disease*, New England Journal of Medicine, 331(1), 1994, 496-501.

[2] M. Haude, R. Erbel, H. Issa, & J. Meyer, *Quantitative Analysis of Elastic Recoil After Balloon Angioplasty and After Intracoronary Implantation of Balloon-Expandable Palmaz-Schatz Stents,* Journal of the American College of Cardiology, 21(1), 1993, 26-34.

[3] P. W. Serruys, P. De Jaegere, & F. Kiemeneij, *Comparison of Balloon-Expandable-Stent Implantation with Balloon Angioplasty in Patients with Coronary Heart Disease*, New England Journal of Medicine, 331(1), 1994, 489-495.

[4] J. Garasic, E. R. Elazer, J. C. Squire, P. Seifert, M. Williams, & C. Rogers, *Stent and Artery Geometry Determine Intimal Thickening Independent of Arterial Injury*, Circulation, 101(1), 2000, 812-818.

[5] J. F. LaDisa, L. E. Olson, R. C. Molthen, D. A. Hettrick, P. F. Pratt, M. D. Hardel, J. R. Kersten, D. C. Warltier, & P. S. Pagel, *Alterations in Wall Shear Stress Predict Sites of Neointimal Hyperplasia After Stent Implantation in Rabbit Iliac Arteries*, American Journal of Physiology, 288(1), 2005, H2465-H2475.

[6] A. Kastrati, & J. Mehilli, *Restenosis After Coronary Placement of Various Stent Types*, American Journal of Cardiology, 87(1), 2001, 34-39.

[7] H. Jung, J. W. Choi, & C. G. Park, *Asymmetric Flows of Non-Newtonian Fluids in a Symmetric Stenosed Artery*, Korea-Australia Rheology Journal, 16(1), 2004, 101-108.

[8] L. Waite, *Biofluid Mechanics in Cardiovascular Systems* (NY: McGraw-Hill, 2006).

[9] C. Rogers, & E. R. Edelman, *Endovascular Stent Design Dictates Experimental Restenosis and Thrombosis*, Circulation, 91(1), 1995, 2995-3001.

[10] A. M. Malek, S. L. Alper, & S. Izumo, *Hemodynamic Shear Stress and its Role in Atherosclerosis*, Journal of the American Medical Association, 282(21), 1999, 2035-2042.

[11] T. Seo, L. Schachter, & A. Barakat, *Computational Study of Fluid Mechanical Disturbance Induced by Endovascular Stents,* Annals of Biomedical Engineering, 33(4), 2005, 444-456.

[12] C. Brown, *Morphological, Biochemical, and Functional Changes in Human Platelets Subjected to Shear Stress*, Journal of Laboratory and Clinical Medicine, 86(1), 1975, 462-471.

[13] T. Asahara, C. Bauters, C. Pastore, & M. Kearney, *Local Delivery of Vascular Endothelial Growth Factor Accelerates Re-endothelialisation and Attenuates Intimal Hyperplasia in Balloon-Injured Rat Carotid Artery*, Circulation, 91(1), 1995, 2793-2801.

[14] N. DePaola, M. Gimbrone, P. F. Davies, & C. F. Dewey, *Vascular Endothelium Responds to Fluid Shear Stress Gradients*, Arteriosclerosis and Thrombosis, 12(1), 1992, 1254-1257.

[15] A. J. Lansky, G. S. Roubin, C. B. O'Shaughnessy, P. B. Moore, & L. S. Dean, *Randomized Comparison of the GR-II Stent and Palmaz-Schatz Stent for Elective Treatment of Coronary Stenoses,* Circulation, 102(1), 2000, 1364-1368.